

PAPER PRESENTED AT 28TH EU PVSEC, PARIS, FRANCE, 2013

100-period, 1.23-eV bandgap InGaAs/GaAsP quantum wells for high-efficiency GaAs solar cells: toward current-matched Ge-based tandem cells

Hiromasa Fujii^{1*}, Kasidit Toprasertpong¹, Yunpeng Wang², Kentaroh Watanabe², Masakazu Sugiyama¹ and Yoshiaki Nakano^{1,2}

¹ Department of Electrical Engineering and Information Systems, The University of Tokyo, Tokyo, Japan

² Research Center for Advanced Science and Technology, The University of Tokyo, Tokyo, Japan

ABSTRACT

Major challenges for InGaAs/GaAsP multiple quantum well (MQW) solar cells include both the difficulty in designing suitable structures and, because of the strain-balancing requirement, growing high-quality crystals. The present paper proposes a comprehensive design principle for MQWs that overcomes the trade-off between light absorption and carrier transport that is based, in particular, on a systematical investigation of GaAsP barrier effects on carrier dynamics that occur for various barrier widths and heights. The fundamental strategies related to structure optimization are as follows: (i) acknowledging that InGaAs wells should be thinner and deeper for a given bandgap to achieve both a higher absorption coefficient for 1e-1lh transitions and a lower compressive strain accumulation; (ii) understanding that GaAs interlayers with thicknesses of just a few nanometers effectively extend the absorption edge without additional compressive strain and suppress lattice relaxation during growth; and (iii) understanding that GaAsP barriers should be thinner than 3 nm to facilitate tunneling transport and that their phosphorus content should be minimized while avoiding detrimental lattice relaxation. After structural optimization of 1.23-eV bandgap quantum wells, a cell with 100-period In_{0.30}GaAs(3.5 nm)/GaAs(2.7 nm)/GaAsP_{0.40}(3.0 nm) MQWs exhibited significantly improved performance, showing 16.2% AM 1.5 efficiency without an anti-reflection coating, and a 70% internal quantum efficiency beyond the GaAs band edge. When compared with the GaAs control cell, the optimized cell showed an absolute enhancement in AM 1.5 efficiency, and 1.22 times higher efficiency with 38% current enhancement with an AM 1.5 cut-off using a 665-nm long-pass filter, thus indicating the strong potential of MQW cells in Ge-based 3-J tandem devices. Copyright © 2013 John Wiley & Sons, Ltd.

KEYWORDS

quantum well solar cells; Strain compensation; III–V compound semiconductor; carrier collection efficiency

*Correspondence

Hiromasa Fujii, Department of Electrical Engineering and Information Systems, The University of Tokyo, Tokyo, Japan.

E-mail: fujii@hotaka.t.u-tokyo.ac.jp

Received 27 June 2013; Revised 30 October 2013; Accepted 12 November 2013

1. INTRODUCTION

As one of the most successful third-generation photovoltaic concepts [1], III–V compound multi-junction solar cells [2–4] have been the focus of intense research towards achieving ultra-high energy conversion efficiency in excess of the Shockley–Queisser Limit [5]. Among the various tandem design structures, InGaP/GaAs/Ge lattice-matched triple-junction cells have been widely used for terrestrial photovoltaics under light concentration conditions [6,7], in addition to space applications [8,9]. However, cell efficiency with this conventional material combination is

limited by the current mismatch problem resulting from the wide GaAs bandgap, and further efficiency enhancement is being pursued by efforts to extend the absorption edge of the middle cell to approximately 1000 nm. While lattice mismatched metamorphic structures using InGaAs as the middle cell material have achieved among the highest efficiencies (exceeding 40%) to date, the use of graded buffer layers just a few micrometers thick is indispensable for preventing lattice relaxation during crystal growth [10–12].

The InGaAs/GaAsP strain-compensated multiple quantum wells (MQWs) are promising narrow-bandgap materials that can be pseudo-lattice-matched to Ge or GaAs [13]. By

alternately growing InGaAs absorber layers with compressive strain and GaAsP strain-balancing layers with tensile strain on nanometer-scale, a large number of MQWs can be epitaxially grown on GaAs. The targeted bandgap of 1.20–1.25 eV, including quantum confinement effects, can be obtained by adjusting the composition and the thickness of each layer. Incorporation of such MQWs or superlattice structures has been proposed not only for current-matched tandem solar cells but also for high-efficiency single-junction solar cells [14,17].

Although the potential of InGaAs/GaAsP MQW solar cells has been experimentally demonstrated in terms of improvement in device performance, understanding of physics in quantum structures, and implementation of MQW into tandem devices [15,16,18,19], challenges still exist from the viewpoints of both crystal growth and structural design toward practical application. The growth challenge is primarily attributed to the difficulty in controlling the strain balance, especially in crystals with high indium and phosphorus contents, where lattice relaxation gradually occurs during formation of the hetero-interface between the two oppositely strained layers. This results in severe crystal degradation as a large number of layers are grown, even though, in theory, MQWs can be epitaxially stacked infinitely if the compressive and tensile strain completely balance each other out [20,21].

The difficulty in achieving a suitable structural design is due to the trade-off between light absorption and carrier collection, which is a general challenge not only for InGaAs/GaAsP MQWs but also other material systems [22–24]. For complete absorption of photons with energies above the effective bandgap of the MQW, the excitations involving ground-state electrons and holes, that is, 1e-1hh transitions, must be sufficiently large. This necessity, however, requires a large number of wells to be stacked, which imposes more difficulty in extracting carriers through the MQW regions because of the weakened electric field in the thickened i-region. To overcome this transport problem, various strategies based on MQW structural design have been proposed. These include using a superlattice with ultra-thin barriers to facilitate tunneling [25], limiting the number of thick wells to suppress non-radiative recombination [26], using step-designed MQWs for efficient thermionic carrier escape [27], and performing quick carrier extraction from deep wells via resonant-tunneling-assisted processes [28].

introduced MQWs with band-edge limits of 950 nm, or periods below 70. In contrast, the present paper proposes a comprehensive design principle for MQW structures that achieve more efficient light absorption and carrier collection while also facilitating successful crystal growth. As a result of quantum structure optimization, absolute enhancement of AM 1.5 efficiency with 100-period MQWs with a band edge of 1008 nm has been achieved.

2. DESIGN PRINCIPLE

The InGaAs/GaAsP quantum wells in general use are composed of InGaAs well layers, GaAsP barrier layers, with GaAs interlayers between them. Here, the GaAs interlayers are optional, and the band for a single well has a stepped structure for relatively thick interlayers, whereas it has a rectangular line-up in the absence of interlayers. The proposed design principle in this paper can be summarized into the following three points:

- InGaAs wells should be made thinner and deeper for a given bandgap in order to achieve both a higher absorption coefficient for 1e-1hh transitions, and to reduce the compressive strain accumulation.
- GaAs interlayers with thicknesses of just a few nanometers can effectively extend the absorption edge to longer wavelengths without introducing compressive strain, and can also suppress lattice relaxation during growth.
- GaAsP barriers should be thinner than 3 nm to facilitate tunneling transport, and their phosphorus content should be minimized while avoiding detrimental lattice relaxation.

In the rest of this section, the theoretical and experimental grounds for this proposed design principle will be discussed, with significant focus paid to the GaAsP barrier design, which is the most important aspect of the structural optimization required for efficient carrier transport.

2.1. InGaAs well design

The light absorption coefficient due to direct transitions in quantum wells can be written as

$$\alpha_{\text{QW}}(E) = \frac{e^2 \hbar |M_0|^2}{L_{\text{W}} m_0^2 \varepsilon_0 c n E} \left(\frac{\mu}{\hbar^2} \right) \cdot \sum_n \Theta(E - E_{\text{QW},n}) [F_{\text{V},n}(E) - F_{\text{C},n}(E)] \quad (1)$$

Yet, despite the progress that has been made against these challenges, successful demonstration of InGaAs/GaAsP MQW cells with a band edge extended beyond 1000 nm, and over 100 periods, has yet to be reported. To date, most research efforts related to this material system have

where e is the elementary charge, M_0 is the momentum matrix element, μ is the reduced mass of electrons and holes, L_{W} is the well thickness, m_0 is the electron static mass, ε_0 is the vacuum permittivity, c is the light velocity, n is the refractive index of the cell material, and Θ is a step

function representing the density of states [29]. $E_{QW,n}$ is the n -th quantized transition energy, which is the sum of the bandgap of the well material and the eigen-energies in the conduction and valence bands. $F_{C,n}$ and $F_{V,n}$ are the distribution functions for each quantum level for electrons and holes, respectively.

The absorption coefficient at a specific wavelength is given as a sum for the available transitions, and the light absorption becomes least efficient in the wavelength range where only 1e-1hh transitions can occur. Therefore, enhancing transitions between the ground states is essential for complete absorption of photons with energies above the MQW bandgap. As shown in Equation (1), the absorption coefficient for each transition is inversely proportional to L_W , and thus the absorbance of one quantum well, which is the product of the well thickness and the absorption coefficient, is maintained for each transition even if the thickness differs. In the entire MQW region, consequently, the absorption contribution from the 1e-1hh transitions is determined by the number of wells, regardless of the well thickness. For a given bandgap, therefore, incorporation of a larger number of thinner wells is a principle strategy in terms of efficient absorption in an i-region, the thickness of which should be minimized for more efficient carrier collection. Note that the wells must be made deeper to maintain the effective bandgap at a longer wavelength because of the stronger quantum confinement effects present in thinner wells.

Thin and deep InGaAs wells also offer advantages with regard to crystal growth. Accumulation of compressive strain per single InGaAs layer is smaller for a thin and deep well with a high indium content than that for a wide and shallow well. Figure 1 shows simulated InGaAs well thickness and accumulated compressive strain per well as functions of indium content for InGaAs/GaAs quantum wells with an absorption-edge energy of 1.23 eV. The absorption-edge energy in quantum wells is defined as

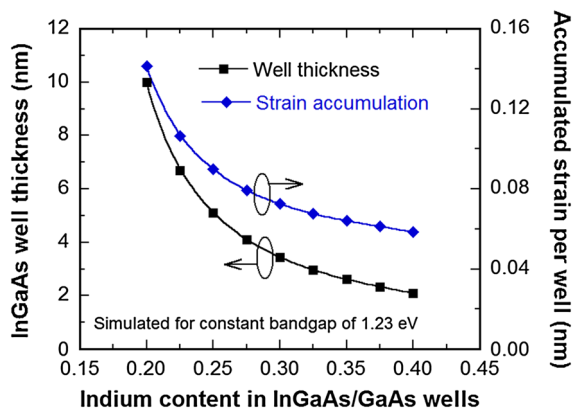


Figure 1. Simulated InGaAs well thickness and accumulated compressive strain per well as a function of indium content for 1.23-eV bandgap InGaAs/GaAs quantum wells. Accumulated strain (nm) is calculated as the product of the lattice mismatch in the InGaAs and the well thickness.

the sum of the bulk bandgap of the InGaAs layer and the eigen-energies for electrons and heavy holes in their ground states. Therefore, the well thickness necessary to achieve a bandgap of 1.23 eV is uniquely determined for each indium composition. The accumulated compressive strain per InGaAs layer can be then calculated as the product of the lattice mismatch and the well thickness. By increasing the indium content from 20% to 30%, the necessary well thickness and strain accumulation can be reduced approximately by 1/2 and 1/3, respectively. However, if the indium content is too high, it may lead to three-dimensional (3D) growth because of the very thin critical thickness [30,31]. Therefore, an appropriate indium content level should be chosen to avoid abnormal growth occurring.

2.2. GaAs interlayer design

Insertion of GaAs interlayers that are just a few nanometers thick between the InGaAs wells and the GaAsP barriers is an effective way to improve the crystal quality of the MQWs, especially those with high indium and phosphorus contents. A strain-neutral interlayer makes the interface less sharp and suppresses the lattice relaxation caused by the abrupt strain change at interfaces [20]. Figure 2(a) shows high-resolution X-ray diffraction (XRD) patterns for 10-period $\text{In}_{0.30}\text{GaAs}(4.2\text{ nm})/\text{GaAs}/\text{GaAsP}_{0.75}(3.3\text{ nm})$ MQWs grown on GaAs (001) substrates with a variety of GaAs interlayer thicknesses. Without interlayers, no fringe peaks that could be attributed to the superlattice were observed, thus indicating that a periodic structure with controlled layer thicknesses was not formed. In contrast, fringe peaks in the XRD pattern became sharper and stronger when thicker GaAs interlayers were present. The full width at half maximum (FWHM) for the second fringe peak at around -7000 arcsec was 785, 550, and 270 arcsec for interlayer thicknesses of 1.12, 1.68, and 2.24 nm, respectively. The theoretical FWHM without lattice relaxation is 263 arcsec, thus indicating that good crystal quality is obtained with 2.24-nm-thick interlayers. Note that the interlayer thickness required to achieve acceptable crystal quality depends strongly on the indium or phosphorus content and that thicker interlayers are generally needed for larger differences in strain between the InGaAs compressive layer and the GaAsP tensile layer. Therefore, the optimum thickness of the interlayer necessary for successful growth should be determined based on the composition of the MQW structure.

The GaAs interlayers are also beneficial for reducing the effective bandgap by weakening the quantum confinement effect. While thicker wells alone can reduce the bandgap, they simultaneously increase the accumulated compressive strain. Figure 2(b) shows the measured bandgap for $\text{In}_{0.3}\text{GaAs}(3.5\text{ nm})/\text{GaAs interlayer}/\text{GaAsP}_{0.5}(4.0\text{ nm})$ MQWs grown on GaAs substrates with various interlayer thicknesses. Here, it can be seen that GaAs layers that are just a few nanometers in thickness

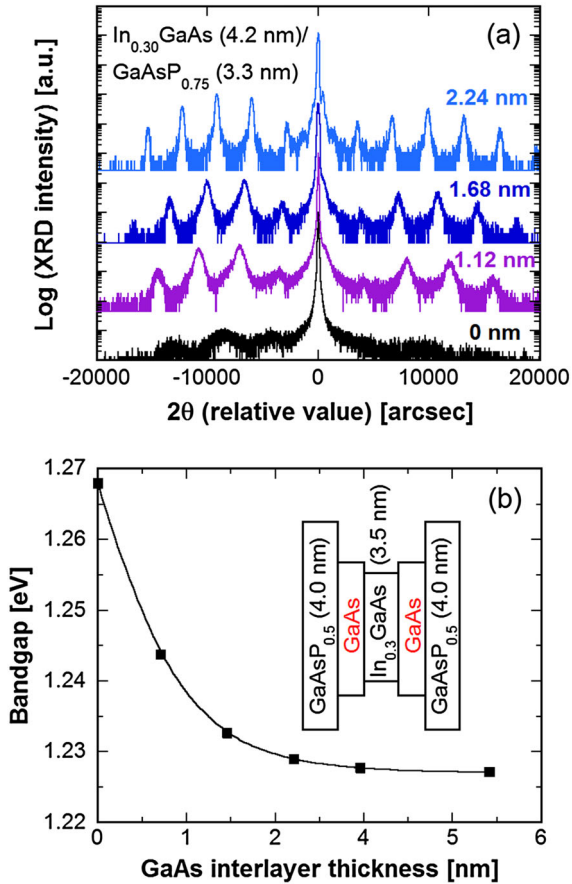


Figure 2. Effects of GaAs interlayers in InGaAs/GaAsP multiple quantum wells (MQWs). (a) X-ray diffraction patterns for 10-period In_{0.30}GaAs(4.2 nm)/GaAs/GaAsP_{0.75}(3.3 nm) MQWs with different GaAs interlayer thickness from 0 to 2.24 nm. (b) Effective bandgap for In_{0.3}GaAs(3.5 nm)/GaAs interlayer/GaAsP_{0.5} (4.0 nm) MQWs versus interlayer thickness. The bandgap was estimated by photoluminescence measurements.

successfully reduce the bandgap by 30–40 meV. Therefore, a practical way to optimize the well structure is to determine the InGaAs thickness required to achieve the desired bandgap and using the highest indium content possible with 2- or 3-nm-thick GaAs interlayers. Note that an interlayer that is too thick may thicken the entire MQW region without providing any additional benefits in terms of crystal quality improvement and/or bandgap reduction.

It is also important to note that GaAs interlayers that are more than just a few nanometers thick prevent carriers in the InGaAs regions from being transported to the neighboring wells via direct tunneling. This can make it difficult to achieve both high crystal quality and efficient carrier transport. However, by thinning the GaAsP layers sufficiently, carriers in InGaAs wells can be thermally transported to the GaAs interlayers where they can then tunnel through the GaAsP barriers, as will be shown in the next section.

2.3. GaAsP barrier design

The GaAsP barrier design has a very significant impact on carrier transport efficiency. The most important requirement is ensuring that tunneling transport through the barrier layers is efficient. However, only a few studies have reported the effects of barrier layers with precisely controlled MQW structures on cell performance [32], and the design criteria necessary to sufficiently extract both photo-excited electrons and holes have yet to be well established. Later in this section, we discuss our experimental investigations into the influence of GaAsP barriers with different widths and heights on the carrier transport dynamics.

2.3.1. Evaluation of carrier collection efficiency.

To characterize the carrier dynamics in MQW cells in detail, we evaluated the cell performance using the carrier collection efficiency (CCE). In this study, the CCE is defined as the fraction of carriers that are actually extracted as a photocurrent divided by the total number of photo-excited carriers in the active region of the cell. This can be calculated by normalizing the illumination-induced current enhancement to its saturation value at reverse bias [33]. To ensure a comprehensive investigation of the cell performance, we carried out CCE evaluations for both AM 1.5 and monochromatic illumination. The CCE under AM 1.5 excitation, CCE_{AM 1.5}, was calculated as

$$CCE_{AM1.5}(V) = \frac{J_{AM1.5}(V) - J_{dark}(V)}{[J_{AM1.5} - J_{dark}]_{sat}} \quad (2)$$

where J_{dark} is the dark current density, $J_{AM 1.5}(V)$ is the J - V characteristics under AM 1.5 illumination, and the denominator term is the saturated value of the current enhancement at reverse bias. CCE_{AM 1.5} gives the total collection efficiency of the carriers excited by sunlight and hence macroscopically indicates how well the cell performs under operational conditions in terms of carrier transport. The monochromatic CCE, CCE(λ , V), on the other hand, was estimated as

$$CCE(\lambda, V) = \frac{J_{mono+AM1.5}(\lambda, V) - J_{AM1.5}(V)}{[J_{mono+AM1.5}(\lambda) - J_{AM1.5}]_{sat}} \quad (3)$$

where $J_{mono+AM 1.5}(\lambda, V)$ is the current density under AM 1.5 illumination with an additional 2.5 mW/cm² monochromatic light at a wavelength of λ . The reason for using AM 1.5 as bias light is that carrier behavior under strong sunlight illumination differs from that under weak monochromatic illumination conditions [33], and bias sunlight is necessary in order to accurately evaluate the carrier dynamics in actual cell operation.

The advantage of a CCE investigation is that, providing the effects of series resistance are sufficiently small, it selectively examines the extraction of photo-excited carriers almost independently of the diode characteristic. Such information cannot be obtained via the typical

characterizations applied to solar cell devices, such as comparison of the zero-bias quantum efficiency (QE) or the I - V curve under sunlight.

Additionally, the monochromatic CCE allows us to manipulate the carrier generation distribution in the depth direction by changing the irradiation wavelength, and consequently examine the difficulty of carrier collection from each area in the device. Furthermore, applying a forward voltage weakens the electric field in the i-region and prevents carrier escape from the wells, thus resulting in a lower CCE. Therefore, by combining the bias- and wavelength-dependent CCE analyses, we can quantitatively estimate how efficiently carriers are extracted during cell operation.

2.3.2. Effects of barrier width and height on carrier transport.

To systematically investigate the effects of barrier design on carrier transport, we prepared a set of GaAs pin cells including 30-period In_{0.3}GaAs(3.5 nm)/GaAs(2.6 nm)/GaAsP MQWs in the i-region at a variety of barrier thicknesses (2–6 nm) and phosphorus contents (40–60%). The i-region thickness was kept constant at 1000 nm for all the devices by adjusting the thickness of the intrinsic GaAs spacer layers beneath the MQW region in order to ensure a constant built-in field. Additionally, the thickness of the i-GaAs spacer layer above the MQW region was fixed at 200 nm to ensure that the intensity of the incident light penetrating the top of the MQW region was equal among the various cells. However, the strain-balance condition was not completely met in most of the samples, as only the GaAsP layer structure was changed. Nevertheless, *ex situ* XRD reciprocal space mapping showed that lattice relaxation resulting from strain accumulation was negligible; the fringe peaks around the (224) diffraction point attributed to the superlattice were well aligned along the vertical axis in the reciprocal space for all the MQW structures. The photoluminescence peak wavelengths were 1006 ± 1 nm regardless of the barrier design, indicating a constant effective bandgap of approximately 1.23 eV. Note that the devices were p-on-n structures, and the p-side of the cells was irradiated by light.

Figure 3(a) shows $CCE_{AM1.5}$ as a function of the voltage for various (2–6 nm) GaAsP barrier thicknesses and with a fixed phosphorus composition of 50%. Because the strain compensation condition was met with 4-nm barriers, MQWs with 2- to 3- and 5- to 6-nm barriers had compressive and tensile strain accumulations, respectively. As the barrier thickens, carrier transport becomes dominated by slow thermionic escape, which lowers the CCE below 100%, even under short-circuit conditions for 5- and 6-nm barriers. This effect appeared more significantly at forward bias with a weak electric field in the i-region, and the 4-nm barrier sample also showed gradual CCE degradation. Regarding the I - V characteristics, poor carrier collection primarily affected the fill factor (FF), which was 0.75 and 0.79 for 6 and 2 nm, respectively. No significant bias dependence of the $CCE_{AM1.5}$ was

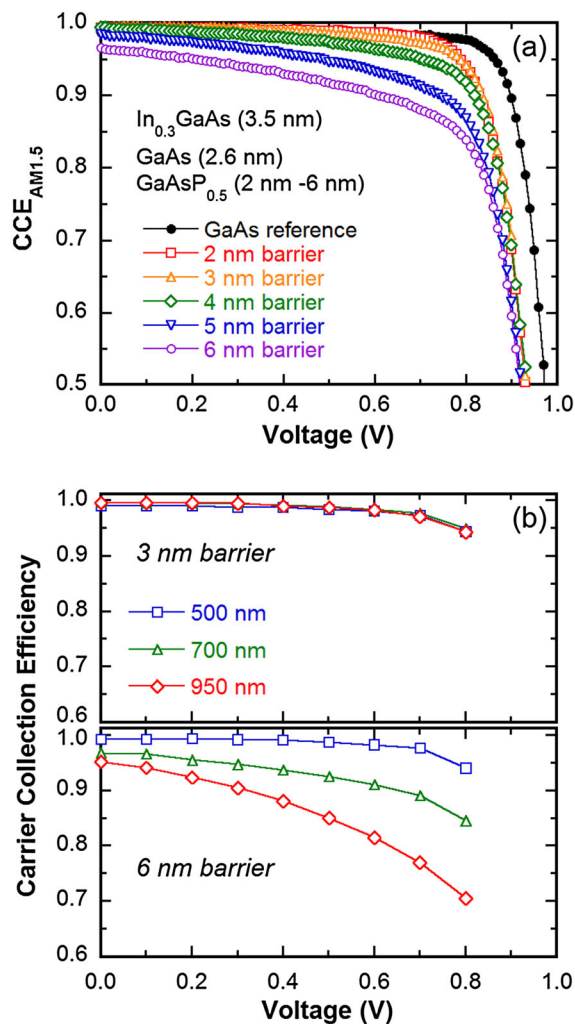


Figure 3. Effects of GaAsP barrier thickness on carrier transport in 30-period In_{0.3}GaAs(3.5 nm)/GaAs(2.6 nm)/GaAsP_{0.5} multiple quantum well cells. (a) Carrier collection efficiency (CCE) under AM 1.5 as function of applied bias with various barrier thicknesses from 2 to 6 nm. Data for GaAs reference cell is shown for comparison. (b) Monochromatic CCE for 2- and 6-nm barriers at excitation wavelengths of 500, 700, and 950 nm.

found for barriers thinner than 3 nm, thus indicating sufficient facilitation of tunneling transport. The $CCE_{AM1.5}$ at the maximum power output voltage of 0.81 V for the GaAs reference cell, 0.73 V for the 3-nm barrier cell, and 0.76 V for the 6-nm barrier cell was 98%, 97%, and 87%, respectively. As a result, carrier transport in the 3-nm-thick barrier cell was found to be as efficient as that in the GaAs bulk reference cell.

In order to determine the mechanism of the enhanced CCE with thinner barriers in greater detail, the monochromatic CCE was examined at 500, 700, and 950 nm with the 3- and 6-nm barrier cells, as shown in Figure 3(b). We found that, because of the high absorption coefficient, 500-nm light is absorbed only in the top p-region, and thus the obtained CCE is solely determined by electron

transport through the MQW region because there is essentially no blockage for hole transport to the top contact. At 700 nm, approximately 40% of the light reaches the MQW region, partially exciting carriers in the MQWs. Therefore, the CCE at 700 nm includes the dynamics of electron-hole separation inside the wells, and the efficiency of hole transport through the MQW to the top p-region. As 950-nm light is only absorbed in the InGaAs wells, the CCE selectively shows the probability of carrier escape from the MQW region. Note that excitation at 950 nm only generates electrons and heavy holes in their ground states because only 1e-1hh transitions are possible at this wavelength.

At a forward bias of 0.7 V, the CCE was degraded at longer wavelengths for the 6-nm barrier and had values of 97%, 89%, and 77% at 500, 700, and 950 nm, respectively. This indicates that the transport of heavy holes, which are photo-generated inside the wells, is more likely to be blocked by thick barriers. This conclusion is reasonable because heavy holes in GaAs-based materials have effective masses that are approximately 10 times larger than that of electrons, and the thermionic escape rate for heavy holes from a well is much lower than that for electrons. In addition, a larger effective mass lowers the confinement energy in a quantum well, and because the ground state of a heavy hole is located close to the bottom of the well, the potential barrier for heavy holes is higher. At 500 nm, the CCEs for the 3- and 6-nm barrier cells were comparable, thus indicating extremely fast electron thermionic escape. On the other hand, the 3-nm barrier cells showed an almost equivalent CCE bias dependence, regardless of the excitation wavelength, with a CCE of 97% at 0.7 V. This is clear evidence that heavy hole transport can be sufficiently enhanced by tunneling with GaAsP barriers as thin as 3 nm.

Figure 4(a) shows the $CCE_{AM\ 1.5}$ at a fixed barrier thickness of 3 nm and various phosphorus contents (40–60%). As can be seen, a very high CCE of approximately 99% was obtained at 0 V regardless of the barrier height (or the phosphorus content) because tunneling transport is well facilitated. However, because of the lower tunneling probability through higher potential barriers, the CCE for samples with higher phosphorus contents decreased drastically as the forward bias increased, resulting in a CCE of 95% and 98% at 0.7 V for a phosphorous content of 60% and 40%, respectively.

As indicated in the graph, increasing the phosphorus content from 40% to 60% increased the difference in the bandgap at the Γ point between GaAs and GaAsP by approximately 0.2 eV, but the effect of the barrier height on the carrier transport is by far smaller than that of the barrier width because tunneling is much more efficient than thermionic processes. Therefore, the influence of the barrier height difference on the J - V characteristics was very small for the five devices observed, and included a slight FF degradation from 0.801 with 40% phosphorus to 0.789 with 60% phosphorus, and no apparent change in J_{sc} or V_{oc} . The degradation in cell performance with

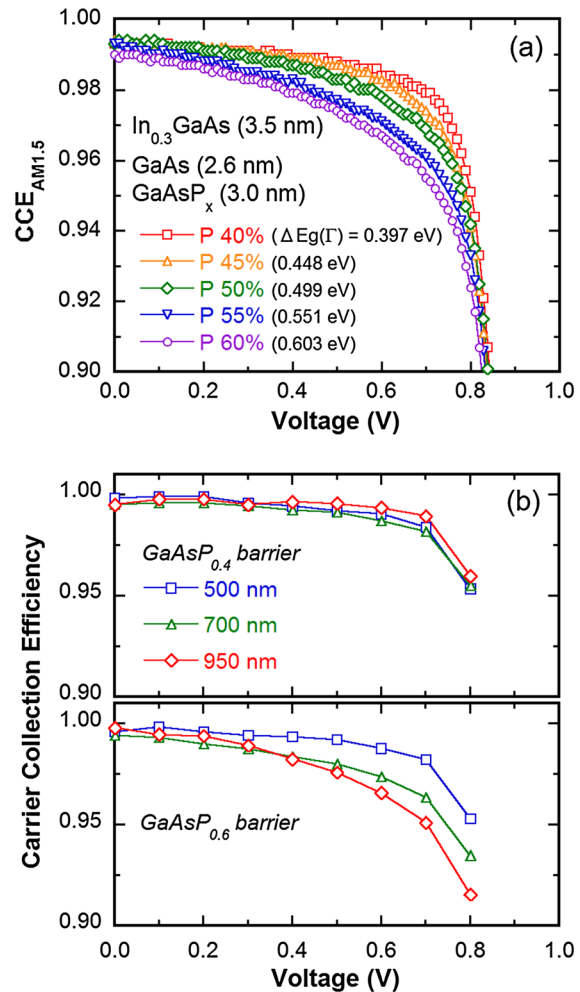


Figure 4. Effects of GaAsP barrier composition on carrier transport in 30-period In_{0.3}GaAs(3.5 nm)/GaAs(2.6 nm)/GaAsP(3.0 nm) multiple quantum well cells. (a) Carrier collection efficiency (CCE) under AM 1.5 as function of applied bias with various phosphorus contents from 40 to 60%. Bandgap difference at the Γ point between GaAs and GaAsP is shown as $\Delta E_g(\Gamma)$. (b) Monochromatic CCE with 40% and 60% phosphorus at excitation wavelength of 500, 700, and 950 nm.

higher barriers, however, should be more apparent when over 100 wells are incorporated, and reducing the phosphorus content in the barriers as much as possible becomes increasingly important as the well number increases.

A CCE investigation under monochromatic illumination conditions was also carried out to determine how higher barriers block carrier transport. Figure 4(b) shows the CCE for MQW cells with 40% and 60% phosphorus at various excitation wavelengths. Here, it can be seen that the CCE with 40% phosphorus showed a similar bias dependence, with a value of over 98% at 0.7 V, regardless of the illumination wavelength, thus indicating equivalent transport efficiency for electrons and holes. On the other hand, at longer wavelengths, obvious degradation was observed for 60% phosphorus, with a CCE of 98%, 96%,

and 95% at 500, 700, and 950 nm, respectively, at the forward bias of 0.7 V. This clearly indicates that the escape of heavy holes is blocked by higher barriers. This is partly because the effective mass of a heavy hole is much larger than that of an electron as previously mentioned. Moreover, the higher phosphorus content in GaAsP generally leads to a larger band offset for the valence band than the conduction band, and hence creates higher potential barriers and a lower tunneling probability for heavy holes.

The previous investigation into carrier behavior in various GaAsP layer structures led us to the principle design criteria that barriers should be no more than 3-nm thick, and that they should have as low a phosphorus content as possible without introducing detrimental lattice relaxation. Although direct tunneling between InGaAs wells is prevented when GaAs interlayers that are just a few nanometers thick are inserted on both sides of GaAsP barriers, facilitating tunneling between neighboring GaAs interlayers was found to be a remarkably effective way of enhancing the carrier transport for the entire device, and this could be accomplished by reducing the barrier thickness to 3 nm and limiting the phosphorus content to 0.4.

3. PERFORMANCE WITH THE OPTIMIZED MQW STRUCTURE

To demonstrate the design strategy discussed previously, structural optimization for an effective bandgap of 1.23 eV was carried out with the MQW structures shown in Table I. Here, we implemented 100-period In_{0.30}GaAs (3.5 nm)/GaAs(2.7 nm)/GaAsP_{0.40}(3.0 nm) quantum wells in a GaAs p-i-n cell as the optimized MQW structure. For comparison purposes, we also prepared a sample with 70-period In_{0.22}GaAs(7.5 nm)/GaAs(0.6 nm)/GaAsP_{0.40} (8.0 nm) MQWs as a typical MQW cell before optimization. The overall MQW regions in both cells were equally 1180 nm in thickness and were incorporated at the center of 1380-nm-thick i-region, and 100-nm-thick intrinsic GaAs spacer layers were inserted at the top and the bottom of the MQWs. A GaAs bulk cell with a 1380-nm-thick i-region without MQWs was also prepared as a reference cell. The bottom n-region and the top p-region of all cells had dopant concentrations of $2 \times 10^{17} \text{ cm}^{-3}$ and $2 \times 10^{18} \text{ cm}^{-3}$ and thicknesses of 400 nm, 200 nm, respectively. The p-region was covered with a 25-nm-thick In_{0.49}Ga_{0.51}P window layer and then capped with a 50-nm-thick highly doped contact layer. Note that an anti-reflection coating (ARC) was not used in this study.

Figure 5 shows XRD patterns for the two MQW cells under investigation. Here, it can be seen that the optimized MQW100 cell had an overall compressive strain (2620 ppm) due to the intentionally lowered phosphorus content in the barrier layers, whereas the strain in the typical MQW70 cell was completely balanced out. Nevertheless, the XRD pattern for the optimized cell exhibited very sharp fringe peaks, which were attributed to a MQW structure with high crystal quality. Typical MQW70 cells also showed sharp fringe patterns in spite of their relatively thin (0.6 nm) GaAs interlayers. This was the result of the low indium content in the wells and hence the smaller difference in strain between the InGaAs and GaAsP layers. For both cells, the fringe peak positions and their relative intensities agreed quite well with the theoretical curve, taking account of the designed structure, thus indicating that the MQW regions were uniformly grown as designed in terms of the composition and the thickness of each layer.

Figure 6 shows the absorbance of the MQW A_{MQW} beyond the GaAs band edge measured by Fourier

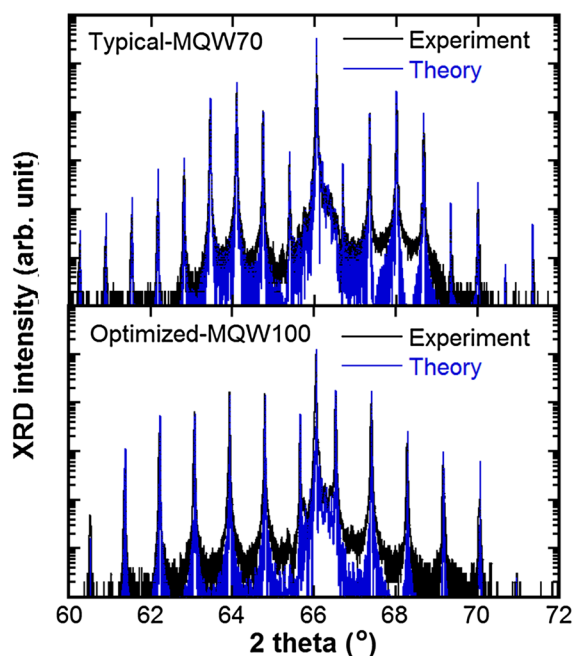


Figure 5. X-ray diffraction (XRD) 2θ - ω pattern for typical multiple quantum well (MQW)70 cell and optimized MQW100 cell around the (004) diffraction peak. Theoretical curves for the designed cell structures are also shown.

Table I. Multiple quantum well (MQW) structures inserted in GaAs pin cells before and after optimization.

Structure (periods)	Well (nm)	Barrier (nm)	Interlayer (nm)
Typical MQW(70)	In _{0.22} Ga _{0.78} As (7.5)	GaAs _{0.60} P _{0.40} (8.0)	GaAs (0.6)
Optimized MQW(100)	In _{0.30} Ga _{0.70} As (3.5)	GaAs _{0.60} P _{0.40} (3.0)	GaAs (2.7)

The numbers in the structure column indicate the number of MQW periods. The total MQW region was approximately 1180 nm thick in both structures. MQWs were inserted in the center of a 1380 nm i-region with 100-nm-thick intrinsic GaAs spacers on the top and the bottom.

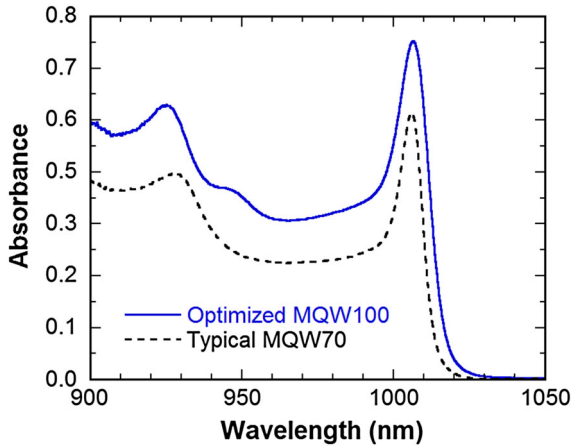


Figure 6. Absorbance of multiple quantum wells (MQWs) measured by Fourier transform infrared spectroscopy before depositing contacts on back surface. Absorbance of the GaAs reference cell without MQWs was used for the background spectrum. Note that the absorbance includes the effects of multiple reflections inside the cells.

transform infrared spectroscopy before processing the surface and back contacts. A_{MQW} was calculated as

$$A_{MQW} = -\log_{10} \left(\frac{T_{\text{sample}}}{T_{\text{reference}}} \right) \quad (4)$$

where T_{sample} and $T_{\text{reference}}$ are the transmittance of the cells with the MQW and the GaAs reference cell, respectively. Note that the absorbance values in the figure include the effects of multiple reflections inside the cells.

The optimized MQW100 cell showed approximately 100/70 times larger absorbance in the 1e-1hh transition wavelength range than the typical MQW70 cell, as theoretically expected from Equation (1), thus proving the absorbance is determined not by the well thickness but by the number of wells. The total thickness of the well region, that is, the product of the InGaAs layer thickness and the period number, was 350 and 525 nm for the optimized MQW100 and typical MQW70 cells, respectively. Therefore, incorporating a larger number of thinner wells is now an experimentally confirmed strategy leading to increased light absorption with a limited total well thickness.

Figure 7(a) shows the $J-V$ curves for the two MQW cells and the GaAs reference cell under AM 1.5 illumination, and the $J-V$ properties including J_{sc} , V_{oc} , FF, and efficiency are summarized in Table II. The typical MQW70 cell showed a larger J_{sc} of 23.3 mA/cm² than the GaAs reference cell (20.9 mA/cm²) because of the

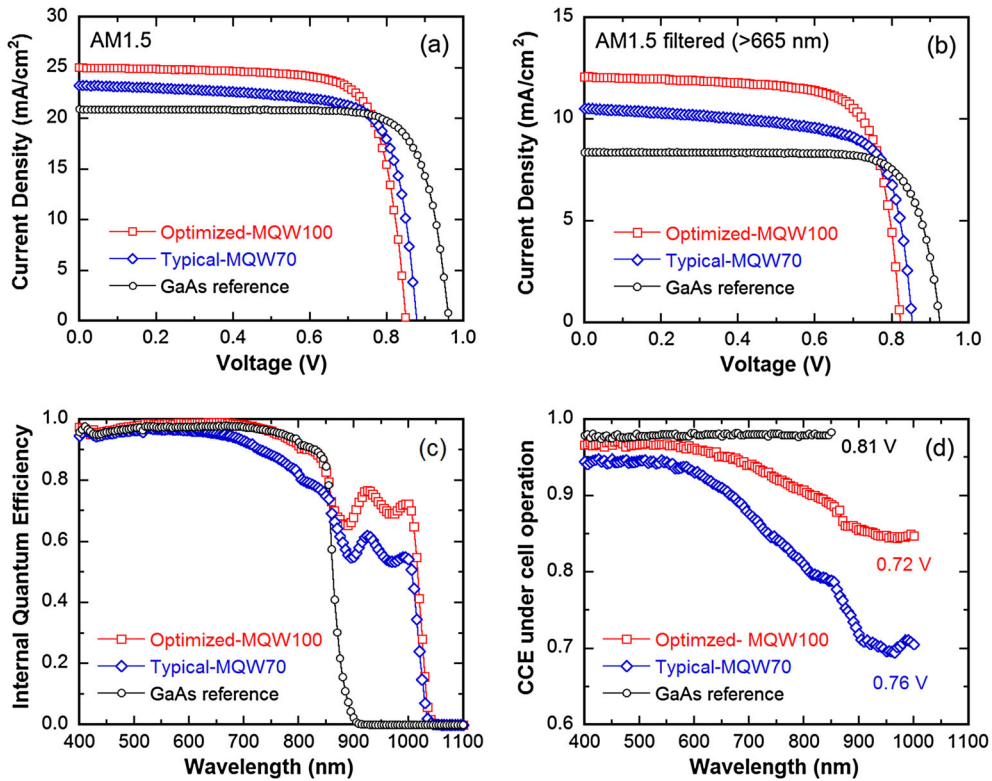


Figure 7. Cell performance for the fabricated photovoltaic devices including $J-V$ characteristics under (a) AM 1.5 illumination and (b) AM 1.5 filtered by a 665 nm long-pass filter (FGL665S, Thorlabs), (c) internal quantum efficiency at 0 V, and (d) wavelength-dependent carrier collection efficiency at maximum power output voltages, which are also shown in the graph. Note that FGL665S transmits approximately 90% of the light beyond 665 nm.

Table II. J - V parameters for the fabricated photovoltaic devices (w/o anti-reflection coating).

	AM 1.5				AM 1.5 filtered (>665 nm)			
	J_{sc} (mA/cm ²)	V_{oc} (V)	FF	Efficiency (%)	J_{sc} (mA/cm ²)	V_{oc} (V)	FF	Efficiency (%)
Optimized MQW100	25.0	0.850	0.761	16.2	12.1	0.823	0.746	14.4
Typical MQW70	23.3	0.879	0.751	15.3	10.5	0.853	0.716	12.5
GaAs ref.	20.9	0.962	0.792	15.9	8.4	0.925	0.784	11.8

Data in the right column were obtained with AM 1.5 cut-off by a long-pass filter (FGL665S, Thorlabs), which transmits approximately 90% of light beyond 665 nm. Note that the efficiency under the filtered AM 1.5 was calculated with a filtered incident illumination energy of 514 W/m².

MQW, multiple quantum well.

infrared response of the MQW. V_{oc} was reduced from 0.96 to 0.88 V, but the drop in eV_{oc} (0.08 eV) was much smaller than the difference in band-edge energy (0.19 eV) between the GaAs control cell and the MQW cell. However, poor carrier transport (due to the lack of tunneling) caused a visible slope in the J - V curve, even at 0 V, resulting in a small FF of 0.75. Accordingly, the AM 1.5 efficiency was lower for the typical MQW70 cell (15.3%) than the GaAs cell (15.9%). Along with an increased well number, the optimized MQW100 cell showed an even larger J_{sc} of 25.0 mA/cm², which was 1.2 times higher than the GaAs reference cell. The J_{sc} enhancement was as large as 4.1 mA/cm² without an ARC. The V_{oc} for the optimized cell was 0.85 V with an approximately 0.03 V drop when compared with the typical MQW70 cell, which may be attributed to slight lattice relaxation caused by the accumulated compressive strain. The V_{oc} drop from the GaAs reference cell was 0.11 V, which was still less than the difference between their effective bandgaps. Furthermore, the optimized MQW100 cell did not show an apparent slope in the J - V curve at 0 V, because of the efficient tunneling made possible by the 3-nm-thick barriers. As a result, the optimized MQW100 cell exhibited a higher FF of 0.76 than the typical MQW70 cell and a higher AM 1.5 efficiency of 16.2% without an ARC, which is 0.3% higher than that for the GaAs reference cell.

Figure 7(b) shows the J - V characteristics under AM 1.5, filtered using a 665 nm long-pass filter (FGL665S, Thorlabs, Newton, New Jersey, USA), which is a more practical performance in a situation where MQW cells are operated as middle cells beneath InGaP top cells. Note that FGL665S transmits approximately 90% of the light beyond 665 nm. Cutting off the short wavelength illumination increases the fraction of the light beyond the GaAs band edge in the incident light and consequently leads to relatively better performance for the cells with MQWs. The short-circuit current for the typical MQW70 and optimized MQW100 cells was increased by 25% and 44%, respectively, from the GaAs reference, resulting in an efficiency enhancement for the MQW cells by a factor of 1.06 and 1.22, respectively. However, the typical MQW70 cell showed a significantly degraded FF due to the insertion of the filter, from 0.75 to 0.71, because of the less efficient extraction of carriers excited at longer wavelength illumination. For the optimized MQW100 cell, on the other hand, such degradation was suppressed, primarily because

of the improved heavy hole transport. As a result, compared with the reference cell, the current enhancement at the maximum power output voltage remained 38% for the optimized MQWs, whereas it was limited to only 13% with the typical MQWs.

Figure 7(c) shows the internal quantum efficiency (IQE) at 0 V. As can be seen, both MQW structures extended the band edge beyond 1000 nm. However, the typical MQW70 cell had an IQE of only 50% beyond the GaAs band edge. It also showed degraded response from 650 to 850 nm compared with the GaAs reference cell because of the poor carrier collection. In contrast, the optimized MQW100 cell had an IQE of over 70% for almost the entire MQW absorption wavelength range, with the response spectrum perfectly matched to the reference cell from 400 to 850 nm.

Evaluation of the CCE at the operation voltage, CCE (V_{max}), is important in terms of practical application. Figure 7(d) shows a comparison of CCE spectra at the maximum output voltages, which were 0.72, 0.76, and 0.81 V for the optimized MQW100 cell, typical MQW 70 cell, and GaAs reference cell, respectively. These spectra can be divided into three wavelength ranges based on the region where the photons are absorbed in the cells: (i) 300–550 nm, (ii) 550–850 nm, and (iii) 850–1000 nm.

At wavelengths below 550 nm, photons are absorbed in the upper area above the MQW region, and thus the CCE is solely determined by electron transport through the *i*-region. Within this short wavelength range, the typical MQW70 cell had a high CCE of 94% despite the lack of quick tunneling transport, because electron thermal escape is efficient, as mentioned previously. In the optimized MQW100 cell, the CCE was further improved to approximately 97%, which was comparable to the value of 98% obtained for the GaAs reference cell, indicating that a 100-period quantum well structure does not block electron transport.

In the wavelength range between 550 and 850 nm, photons can reach the MQW region as well as the upper GaAs regions. If the light penetration to the MQW is shallow, the CCE is primarily determined by electron transport because most carriers are generated in the upper GaAs. As the wavelength becomes longer, the fraction of carriers generated in the wells increases, and the effect of hole transport across the *i*-region becomes larger. The typical MQW70 cell showed a severely degraded CCE at longer wavelengths, indicating poor transport of heavy holes. The optimized MQW100 cell also exhibited a gradual CCE

reduction at longer wavelengths, but it was strongly suppressed because of tunneling transport. The CCE for the GaAs reference remained above 98%, regardless of the excitation wavelength, because of highly efficient transport resulting from the absence of a carrier trapping structure. The effect of slow transport of heavy holes in the typical MQW70 cell was apparent even at 0 V and is reflected in the degraded QE from 650 to 850 nm in Figure 7(c). Heavy hole transport in the optimized MQW100 cell, on the other hand, was still efficient at 0 V, resulting in almost an equivalent QE in the GaAs absorption wavelength range.

Beyond 850 nm, carriers are photo-excited only in the wells and the CCE is determined by the efficiency of heavy hole transport. Therefore, the CCE for the typical MQW70 cell with thick barriers was further degraded to approximately 70%, while the optimized MQW100 cell showed a significantly improved CCE of 85%.

4. CONCLUSIONS

The present paper proposes a general design principle for a suitable quantum well structure that overcomes the major challenges faced by InGaAs/GaAsP MQW solar cells, i.e. the trade-off between light absorption and carrier collection as well as the difficulty in crystal growth of a high-quality MQW consisting of strained layers. The essential strategies for structural optimization are as follows.

- InGaAs wells should be thinner and deeper for a given bandgap to achieve both a higher absorption coefficient for 1e-1hh transitions and lower compressive strain accumulation.
- GaAs interlayers with thicknesses of just a few nanometers are effective for extending the absorption edge to longer wavelengths without additional compressive strain, and for suppressing lattice relaxation during growth.
- GaAsP barriers should be thinner than 3 nm to facilitate tunneling transport, and their phosphorus content should be minimized while avoiding detrimental lattice relaxation.

For barrier design optimization, in particular, the influences of GaAsP layers on the carrier transport were systematically investigated in terms of the CCE with various barrier widths (2–6 nm) and phosphorus contents (40–60%). The transport of heavy holes was found to be the bottleneck especially, in the thermionic escape processes, and making the barriers as thin as 3 nm was found to be an essential criterion for sufficiently facilitating tunneling transport.

After optimization of a MQW structure with the absorption-edge energy of 1.23 eV, a cell with 100-period In_{0.30}GaAs(3.5 nm)/GaAs(2.7 nm)/GaAsP_{0.40}(3.0 nm) MQWs achieved significantly improved performance, showing a 16.2% AM 1.5 efficiency without an ARC, an IQE of 70%

(0 V), and a CCE of 85% (V_{\max}) at wavelengths beyond the GaAs band edge. Compared with the GaAs control cell, the optimized MQW100 cell showed an absolute gain in AM 1.5 efficiency and achieved a 1.22 times higher efficiency with 38% enhancement of the maximum power output current under AM 1.5 cut-off by 665-nm long-pass filter, indicating a strong potential for introduction into Ge-based 3-J tandem devices.

ACKNOWLEDGEMENTS

A portion of this study was supported by the Research and Development of Innovative Solar Cell program, New Energy and Industrial Technology Development Organization (NEDO), Japan.

REFERENCES

1. Green MA. Third generation photovoltaics: ultra-high conversion efficiency at low cost. *Progress in Photovoltaic: Research and Applications* 2001; **9**: 123–135.
2. King RR, Bhusari D, Larrabee D, Liu XQ, Rehder E, Edmondson K, Cotal H, Jones RK, Ermer JH, Fetzer CM, Law DC, Karam NH. Solar cell generations over 40% efficiency. *Progress in Photovoltaics: Research and Applications* 2012; **20**: 801–815.
3. Yamaguchi M, Takamoto T, Araki K. Present and future of super high efficiency multi-junction solar cells. *Proceedings of the SPIE* 2008; **6889**: 688906.
4. Karam NH, King RR, Haddad M, Ermer JH, Yoon H, Cotal HL, Sudharsanan R, Eldredge JW, Edmondson K, Joslin DE, Krut DD, Takahashi M, Nishikawa W, Gillanders M, Granata J, Hebert P, Cavicchi BT, Lillington D. Recent developments in high-efficiency Ga_{0.5}In_{0.5}P/GaAs/Ge dual- and triple-junction solar cells: steps to next-generation PV cells. *Solar Energy Materials & Solar Cells* 2001; **66**: 453–466.
5. Shockley W, Queisser HJ. Detailed balance limit of efficiency of p-n junction solar cells. *Journal of Applied Physics* 1961; **32**: 510–519.
6. Bosi M, Pelosi C. The potential of III-V semiconductors as terrestrial photovoltaic devices. *Progress in Photovoltaics: Research and Applications* 2007; **15**: 51–68.
7. Algora C, Rey-Stolle I, García I, Galiana B, Baudrit M, Espinet P, Barrigón E, González JR. III-V multijunction solar cells for ultra-high concentration photovoltaics. *Proceedings of the IEEE 34th Photovoltaic Specialist Conference*, 2009; 001571–001575.
8. Takamoto T, Kaneiwa M, Imaizumi M, Yamaguchi M. InGaP/GaAs-based multijunction solar cells. *Progress in Photovoltaics: Research and Applications* 2005; **13**: 495–511.

9. Sato S, Ohshima T, Imaizumi M. Modeling of degradation behavior of InGaP/GaAs/Ge triple-junction space. *Journal of Applied Physics* 2009; **105**: 044504.
10. Fetzer CM, King RR, Colter PC, Edmondson KM, Law DC, Stavrides AP, Yoon H, Ermer JH, Romero MJ, Karam NH. High-efficiency metamorphic GaInP/GaInAs/Ge solar cells grown by MOVPE. *Journal of Crystal Growth* 2004; **261**: 341–348.
11. Guter W, Schöne J, Philipps SP, Steiner M, Siefer G, Wekkeli A, Welser E, Oliva E, Bett QW, Dimroth F. Current-matched triple-junction solar cell reaching 41.1% conversion efficiency under concentrated sunlight. *Applied Physics Letters* 2009; **94**: 223504.
12. King RR, Law DC, Edmondson KM, Fetzer CM, Kinsey GS, Yoon H, Sherif RA, Karam NH. 40% efficient metamorphic GaInP/GaInAs/Ge multijunction solar cells. *Applied Physics Letters* 2007; **90**: 183516.
13. Bedair SM, Katsuyama T, Chiang PK, El-Masry NA, Tischler M, Timmons M. GaAsP-GaInAsSb Superlattices: a new structure for electronic devices. *Journal of Crystal Growth* 1984; **68**: 477–482.
14. Barnham KWJ. A new approach to high-efficiency multi-band-gap solar cells. *Journal of Applied Physics* 1990; **67**: 3490–3493.
15. Ekins-Daukes NJ, Barnes JM, Barnham KWJ, Connolly JP, Mazzer M, Clark JC, Grey R, Hill G, Pate MA, Roberts JS. Strained and strain-balanced quantum well devices for high-efficiency tandem solar cells. *Solar Energy Materials & Solar Cells* 2001; **68**: 71–87.
16. Sodabanlu H, Ma S, Watanabe K, Sugiyama M, Yoshiaki N. Impact of strain accumulation on InGaAs/GaAsP multiple quantum wells solar cells: direct correlation between in-situ strain measurement and cell performance. *Japanese Journal of Applied Physics* 2012; **51**: 10ND16.
17. Katsuyama T, Tischler MA, Moore D, Hamaguchi N, Elmasry NA, Bedair SM. New approaches for high efficiency cascade solar cells. *Solar Cells* 1987; **21**: 413–418.
18. Adams JGJ, Browne BC, Ballard IM, Connolly JP, Chan NLA, Loannides A, Elder W, Stavrinou PN, Barnham KWJ, Ekins-Daukes NJ. Recent results for single-junction and tandem quantum well solar cells. *Progress in Photovoltaics: Research and Applications* 2011; **19**: 865–877.
19. Browne B, Lacey J, Tibbits T, Bacchin G, Wu TC, Liu JQ, Chen X, Rees V, Tsai J, Werthen JG. Triple-junction quantum-well solar cells in commercial production. *9th International Conference on Concentrator Photovoltaic Systems*, Miyazaki, 2013.
20. Fujii H, Wang Y, Watanabe K, Sugiyama M, Nakano Y. Suppressed lattice relaxation during InGaAs/GaAsP MQW growth with InGaAs and GaAs ultra-thin interlayers. *Journal of Crystal Growth* 2012; **352**: 239–244.
21. Wang Y, Onitsuka R, Deura M, Yu W, Sugiyama M, Nakano Y. In situ reflectance monitoring for the MOVPE of strain-balanced InGaAs/GaAsP quantum-wells. *Journal of Crystal Growth* 2010; **312**: 1364–1369.
22. Serdiukova I, Monier C, Vilela MF, Freundlich A. Critical built-in electric field for an optimum carrier collection in multiquantum well p-i-n diodes. *Applied Physics Letters* 1999; **74**: 2812–2814.
23. Lynch MC, Ballard IM, Bushnell DB, Connolly JP, Johnson DC, Tibbits TND, Barnham KWJ, Ekins-Daukes NJ, Roberts JS, Hill G, Airey R, Mazzer M. Spectral response and I-V characteristics of large well number multi quantum well solar cells. *Journal of Material Science* 2005; **40**: 1445–1449.
24. Fujii H, Watanabe K, Sugiyama M, Nakano Y. Effect of quantum well on the efficiency of carrier collection in InGaAs/GaAsP multiple quantum well solar cells. *Japanese Journal of Applied Physics* 2012; **51**: 10ND04.
25. Wang Y, Wen Y, Sodabanlu H, Watanabe K, Sugiyama M, Nakano Y. A superlattice solar cell with enhanced short circuit current and minimized drop in open circuit voltage. *IEEE Journal of Photovoltaics* 2012; **2**: 387–392.
26. Welser RE. Thick-well quantum-structured solar cells: design criteria for nano-enhanced absorbers. *Proceedings of the SPIE* 2013; **8620**: 86201C-1.
27. Wen Y, Wang Y, Watanabe K, Sugiyama M, Nakano Y. Effect of GaAs step layer thickness in InGaAs/GaAsP stepped quantum-well solar cell. *IEEE Journal of Photovoltaics* 2013; **3**: 289–294.
28. Alemu A, Freundlich A. Resonant thermo-tunneling design for high performance single junction quantum well solar cells. *IEEE Journal of Photovoltaics* 2012; **2**: 256–260.
29. Fujii H, Wang Y, Watanabe K, Sugiyama M, Nakano Y. High-aspect ratio structures for efficient light absorption and carrier transport in InGaAs/GaAsP multiple quantum well solar cells. *IEEE Journal of Photovoltaics* 2013; **3**: 859–867.
30. Cederberg JG. Self-assembled quantum dot formation during the growth of In_{0.4}Ga_{0.6}As on GaAs(0 0 1) by metal-organic vapor phase epitaxy: the role of In segregation. *Journal of Crystal Growth* 2007; **307**: 44–50.
31. Tan HH, Lever P, Jagadish C. Growth of highly strained InGaAs quantum wells on GaAs substrates—effect of growth rate. *Journal of Crystal Growth* 2005; **274**: 85–89.

32. Toprasertpong K, Fujii H, Wang Y, Watanabe K, Sugiyama M, Nakano Y. Carrier escape time and temperature-dependent carrier collection efficiency of tunneling-enhanced multiple quantum well solar cells. *39th IEEE Photovoltaic Specialist Conference*, Tampa, 2013.
33. Fujii H, Toprasertpong K, Watanabe K, Sugiyama M, Nakano Y. Comprehensive validation of carrier collection efficiency in multiple quantum well solar cells: for more effective and direct evaluation of carrier transport dynamics. *39th IEEE Photovoltaic Specialist Conference*, Tampa, 2013.